Sensors and Actuators A xxx (xxxx) xxx

Contents lists available at ScienceDirect

Sensors and Actuators A: Physical

journal homepage: www.elsevier.com/locate/sna

Usage of the impedance effect of a spiral dual-coil for fingerprint sensor application

Shihwei Lin[b], Mingyu Hsieh[a], Yuanyuan Huang[a], Fuchi Shih[a], Zihsong Hu[a], Weileun Fang[b,c], Chingfu Tsou[a,*]

[a] Department of Automatic Control Engineering, Feng Chia University, Taiwan
[b] Power Mechanical Engineering, National Tsing Hua University, Taiwan
[c] Institute of NanoEngineering and MicroSystems, National Tsing Hua University, Hsinchu, Taiwan

ARTICLE INFO

Article history:
Received 23 April 2019
Received in revised form 16 October 2019
Accepted 9 November 2019
Available online xxx

Keywords:
Dual-coil
Fingerprint
Coupling capacitance

ABSTRACT

This paper presents a design concept that uses the impedance effect of a spiral dual-coil array to identify fingerprint patterns. Unlike commercial optical, resistive, and capacitive sensing technologies, this unique dual-coil design enables the measurement of a fingerprint using the effect of the ridges and valleys on electrical impedance. In this study, a typical sensing chip with a 3×128 dual-coil array was fabricated by a simple microfabrication process. Variations of the coupling capacitance and mutual inductance were then used to verify the properties of different mediums. For a typical case in ambient air, the measured resonant frequency was 8 MHz, which resulted in a maximum induced current of 1.0 mA and a phase shift of 45.5°. The measurement results for saline solutions with different concentrations showed that mediums with higher conductivity caused larger phase shifts. The sample data resulting from the dual-coil array were successfully used to reconstruct a fingerprint image, with a good match in minutiae.

1. Introduction

In the past few decades, there has been a revolution in information technology and the Internet. One of the more important issues that has arisen as a result is cyber security, which has attracted increasing attention for many end users. The use of biometric technology or encryption with terminal systems aiming to identify individual users has become an essential function for many information security management systems. This technology also has unlimited potential for application in medicine and e-business services. Generally, biometric attributes are divided into the two main categories of physiological and behavioral features. Examples of physiological traits are facial, fingerprint, and iris recognition. Behavioral security features focus on the personal behavioral traits of an individual and include voice recognition, gait, and pulse response, etc. [1,2]. Of these approaches, fingerprint recognition is considered the most representative solution for the authentication of individuals in social information systems because of its immutability and because every fingerprint is unique to a particular individual. A wide variety of systems now use this type of biometric security measure, including consumer products such as phones, data storage devices, and notebooks. Compared with other methods, fingerprint sensors are compact, cost effective, easy to use, and power efficient [3,4].

With the rapid development of MEMS and microfabrication technologies, it has become possible to fabricate low-cost chip-based fingerprint sensors with high sensitivity. In principle, fingerprint sensors can be roughly classified as either capacitive [5], optical [6], resistive [7], thermal [8], or ultrasonic [9] sensing types. Each of these sensor types has drawbacks and advantages, as the summarized details in Table 1 [10–15]. A comparison of the sensing performance showed that the drawback of thermal type sensors is that temperature equilibrium between the finger and the sensing element may be reached within a tenth of a second. When such thermal equilibrium occurs, the fingerprint image will disappear and no signal will be induced. Ultrasonic scanners have the advantage of being able to see beneath the skin; however, this technology is slow, expensive, bulky, and too data-intensive for most access control applications. Resistive solutions can suffer from a lack of sensitivity and repeatability due to the temperature effect and hysteresis phenomena of the sensing response. Optical methods may be easily affected by stray light and surface

* Corresponding author.
E-mail address: cftsou@fcu.edu.tw (C. Tsou).

https://doi.org/10.1016/j.sna.2019.111740
0924-4247/

Table 1
Comparison of current fingerprint sensor with their size, response, cost, resolution, and limitation.

Technology	Die size	Response	Power Consumption	Resolution	Limitation
Capacitive	15 × 15 mm^2	150 μs	250 μJ	Less than 600 dpi	Poor performance from contaminated, wet, and damaged finger; suffers from stray capacitance and noise caused by a person
Optical	N/A	N/A	N/A	Less than 500 dpi	Poor image due to dirt, sweet or grease; many components; high power consumption
Piezoresistive	1.28 × 0.2 cm^2	Fast	N/A	Less than 600 dpi	Fatigue failure; protective layer reduces the sensitivity; unsuitable for a full matrix
Thermal	15 × 1500 μm^2	0.1 μs	97.5 W	Less than 600 dpi	Finger image vanished after a short period (less than 1/10 second) due to thermal equilibrium
Ultrasonic	4.73 × 3.24 mm^2	2.64 ms	280 μJ	Up to 1000 dpi	Large size, high cost, and long detection time (few milliseconds)

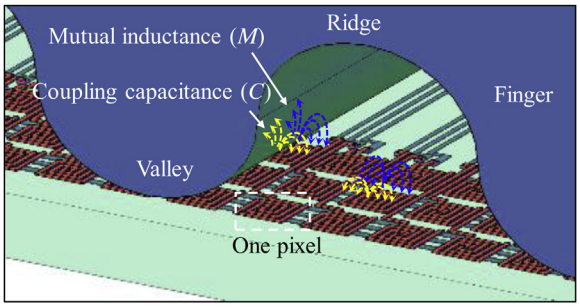

(a)

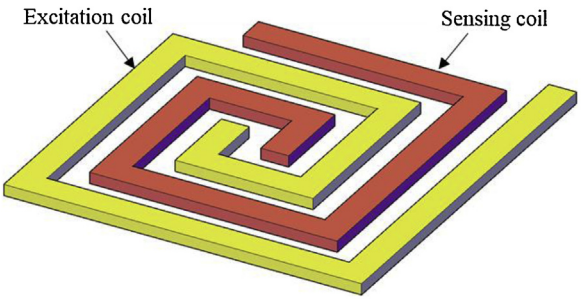

(b)

Fig. 1. a) Fingerprint sensing principle with dual-coil inductance; (b) Schematic view of a spiral co-planar dual-coil.

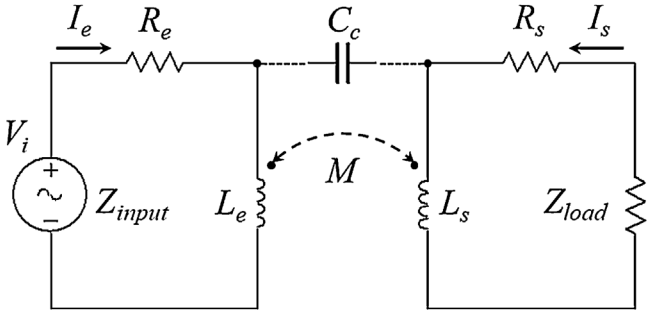

Fig. 2. Simplified equivalent circuit of the dual-coil microstructure.

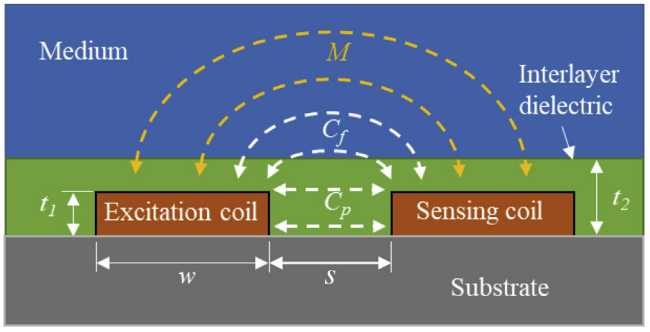

Fig. 3. Schematic cross-section of a dual-coil and the assumed finite boundary of the medium for simulation.

contamination, or possibly even a fingerprint impression left by a prior user. While capacitive sensors are sensitive to electrostatic discharge, although this problem can be resolved conveniently in the circuit detection side. Besides, they are insensitive to liquid mediums, such as perspiration, moisture, and grease, and are more resistant to contamination issues than some optical designs. From these factors, it is clear that a means of reducing the influence of environmental conditions and improving sensing performance are worthy of being developed and would be invaluable to this field.

However, optical and capacitive fingerprint sensors are already widely used in commercial systems and appliances. Therefore, considering the above, this study developed a mutual inductance spiral dual-coil fingerprint sensor, because magnetic inductive technology is only slightly affected by environmental factors (such as humidity or dust), the effect of mechanical loading is small, and the sensors have high sensitivity [16–18]. In addition, the proposed sensing device can be easily fabricated by a simple microfabrication process with three masks. The proposed sensor can recognize a fingerprint's ridges and valleys by identifying the phase differences between excitation and the sensory electrical signals. In this study, the electrical impedance of a spiral dual-coil array and its operating performance were evaluated by experimental measurements. The proposed sensing chip could be used to identify the electrical properties of different mediums in both contact and noncontact situations.

Please cite this article as: S. Lin, M. Hsieh, Y. Huang et al., Usage of the impedance effect of a spiral dual-coil for fingerprint sensor application, Sens. Actuators A: Phys., https://doi.org/10.1016/j.sna.2019.111740

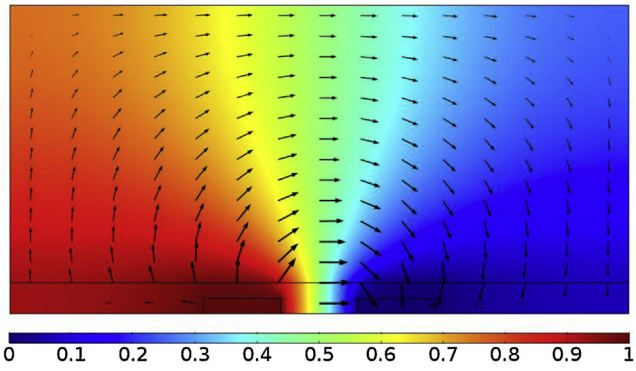

(a)

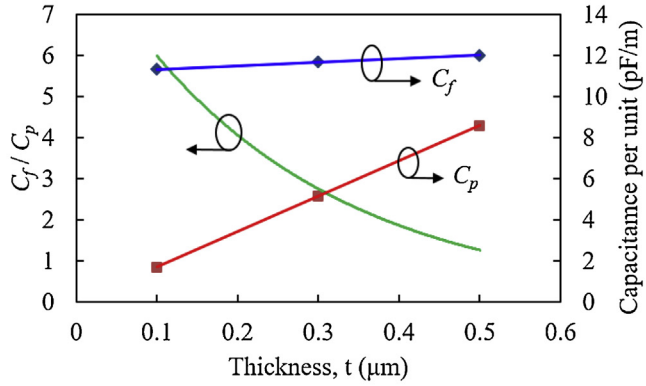

(b)

Fig. 4. a) Typical simulation result for electric field distribution; (b) Parallel capacitance and fringe capacitance variations with the thickness of coil.

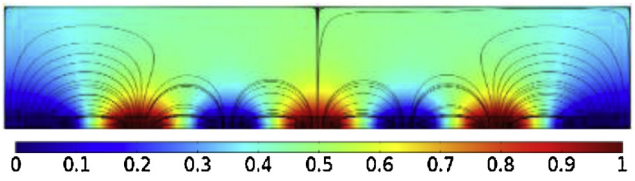

(a)

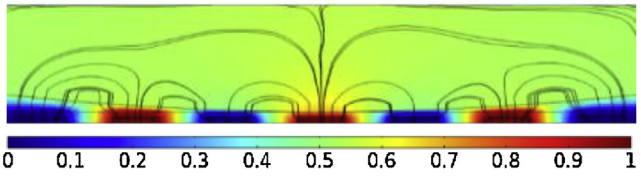

(b)

Fig. 5. Typical simulation results of electric field distribution for mediums in air with different relative permittivity: (a) 1; (b) 80.

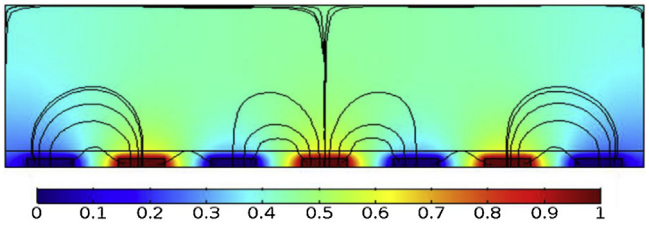

(a)

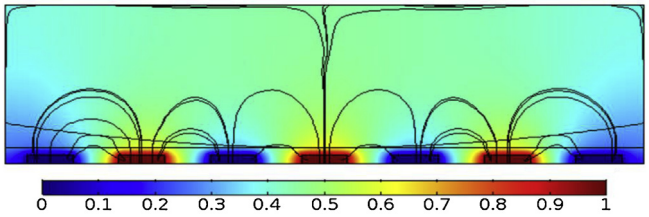

(b)

Fig. 6. Typical simulation results of electric field distribution for mediums in water with different relative permittivity: (a) 78; (b) 80.

2. Design and analysis

2.1. Device design

Based on our previous studies, a novel inspection method that used the mutual inductance of a coplanar dual-coil has been developed to determine the quality of raw milk. When the coils are entirely immersed in raw milk and a specific alternating electrical signal is applied to one of the coils, the other coil induces a phase-shifted electrical signal due to the effect of eddy currents. Using the phase variation between both coils, the quality of the raw milk, in terms of the somatic cell count, can be evaluated [16]. In addition, the sensing performance of different coplanar dual-coil geometries, which affect the phase variation of mutual inductance, is also evaluated [19]. Following above concept, the sensing mechanism for the proposed design, which uses the magnetic inductance of a spiral dual-coil array to reconstruct the image of a fingerprint, is shown in Fig. 1. For each pixel, two individual spiral coils (called the excitation and sensing coils, respectively) are used to produce the coupling capacitance (C) and mutual inductance (M). The transmission of electrical power and signal readout is proceeded by a via contact and metal conductive layer. Therefore, pressing the sensor array with a finger and applying an AC voltage on the excitation coil results in a difference in the coupled electrical properties between the ridges and valleys of the fingerprint. The pixels of the final fingerprint image can be determined in terms of the output signal from the individual dual-coils, such as the phase shift between the excitation and sensing electrical signals.

According to the above, the simplified equivalent circuit for the dual-coil microstructure is shown in Fig. 2, where V_i represents the output voltage of the function generator, R_e and R_s respectively represent the equivalent resistance of the excitation and sensing coils, L_e and L_s respectively represent the equivalent inductance of the excitation and sensing coils, M represents the mutual inductance between both coils, C_c represents the coupling capacitance between the excitation and sensing coils, and Z_{load} represents the output impedance of the circuit. Based on this model and Kirch-

Please cite this article as: S. Lin, M. Hsieh, Y. Huang et al., Usage of the impedance effect of a spiral dual-coil for fingerprint sensor application, Sens. Actuators A: Phys., https://doi.org/10.1016/j.sna.2019.111740

Table 2
The material parameters used in the simulation process.

Materials	Coil (Ni)	Interlayer (SiO_2)	Medium (air)	Medium (water)
Relative permittivity	1000	9.7	1	78
Relative permeability	1240	7	1	1

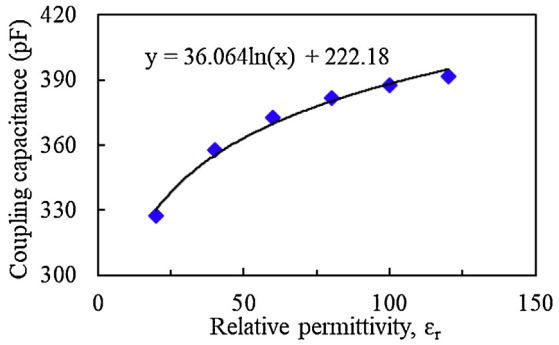

Fig. 7. Variation in the coupling capacitance in air with relative permittivity.

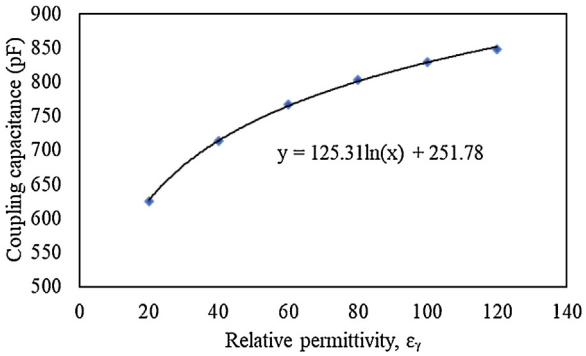

Fig. 8. Variation in the coupling capacitance in water with relative permittivity.

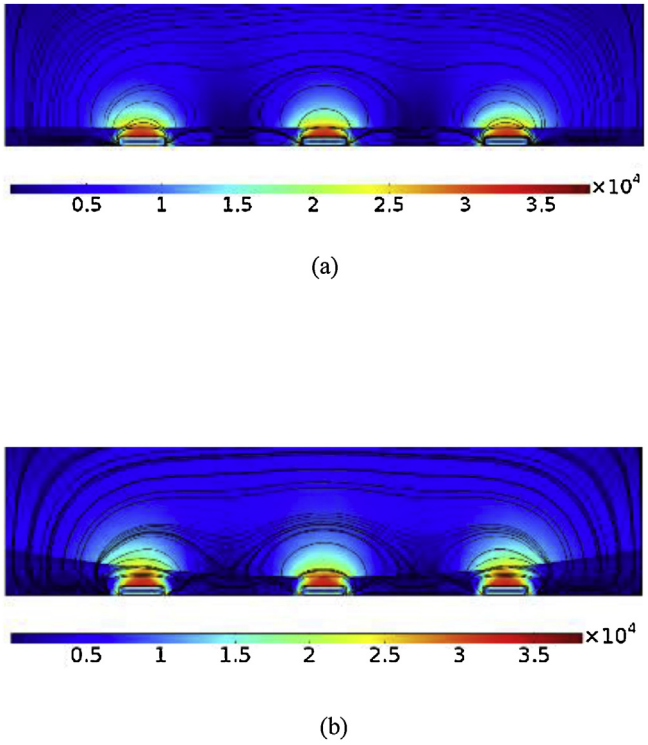

Fig. 9. Typical simulation results of the magnetic field distribution for mediums with different relative permittivity: (a) 1; (b) 0.4.

hoff's circuit laws (KVL), the Z_{load} varies with the driving frequency of the excitation coil and the coupling capacitance between both coils. The resistance and inductance for low frequencies are almost equal to R_e and L_e, respectively. For high frequencies, the inductance settles at a lower value while the resistance settles at a higher value, meaning that the variation of the output signal of the sensing coil under a specific driving frequency is highly dominated by a change in the coupling capacitance and mutual inductance. Therefore, the use of a coplanar dual-coil design with a spiral configuration can increase the coupled effective length in a fixed area. With this benefit, the variations of coupling capacitance and mutual inductances can be increased, resulting in better sensing performance.

2.2. Electrical analysis

The electrical impedance properties of the dual-coil were evaluated using commercial COMSOL simulation software. A 2-D FEM model with a schematic cross-section of a dual-coil and a finite boundary of the medium was first established to simulate the distribution of the coupling capacitance between the excitation and the sensing coils, as shown in Fig. 3. For a typical case, the width (w) and space (s) of the excitation and sensing coils were all set at 5 μm. The thickness (t_1 and t_2) of the coil and the interlayer were 1 μm and 2 μm, respectively, and the height and width of the medium were 18 μm and 40 μm respectively. The assumed material parameters for the simulation are shown in Table 2. In order to simplify the simulation process, the parasitic effects of the substrate were ignored.

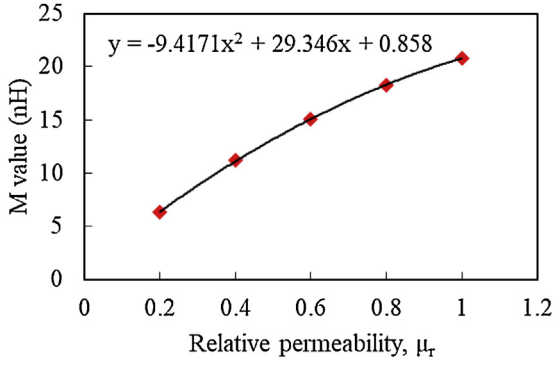

Fig. 10. Variation in the mutual inductance with relative permittivity.

Based on the above conditions, the simulated result for the electric field distribution was as shown in Fig. 4(a) when applying a voltage of 1 V. This result showed that when the point in space was closer to the coil surface, the electric field density would be higher. This implied that when a finger contacted the interlayer dielectric surface, the valley would influence the coupling capacitance more significantly than the ridge. Moreover, the variations of the coupling capacitance were mostly contributed from the change of fringe capacitance C_f, while parallel capacitance C_p was mostly unaffected. Thus, decreasing the coil thickness to increase the ratio between the fringe capacitance and parallel capacitance was an effective way to increase the coupling capacitance variation. As shown in the quantitative simulation result in Fig. 4(b), with differ-

Please cite this article as: S. Lin, M. Hsieh, Y. Huang et al., Usage of the impedance effect of a spiral dual-coil for fingerprint sensor application, Sens. Actuators A: Phys., https://doi.org/10.1016/j.sna.2019.111740

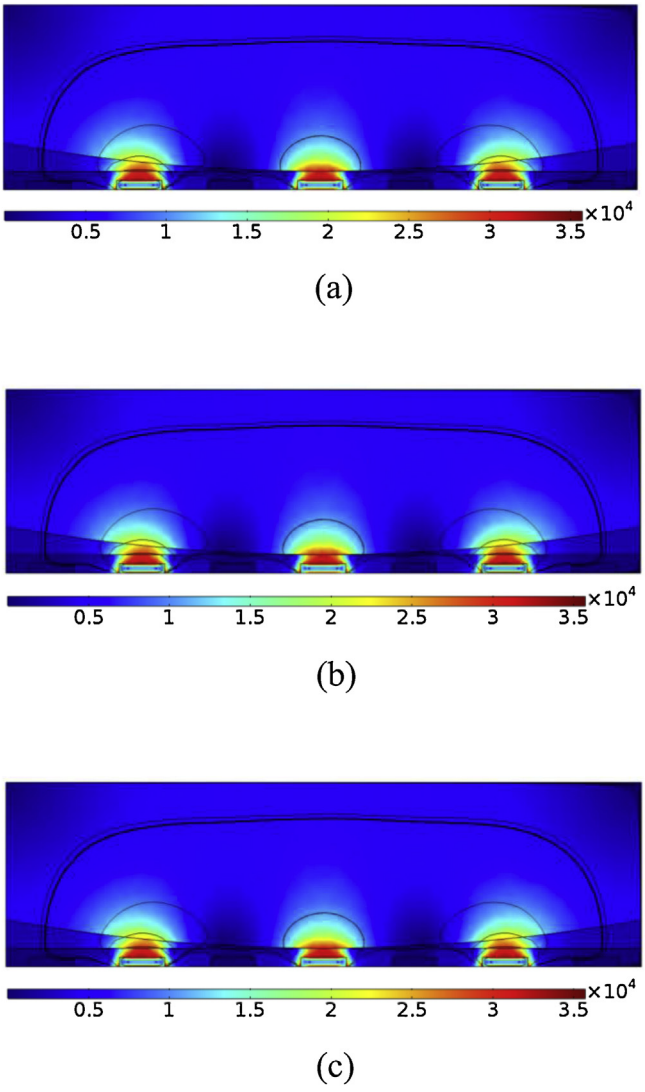

Fig. 11. Typical simulation results of the magnetic field distribution for finger with different resistivity (Ω·m): (a) 1.0; (b) 1×10^2; (c) 1×10^4.

ent coil thicknesses, the ratio C_f / C_p was up to six times when the thickness was 0.1 μm. However, a thinner coil could increase the entire resistance, which would increase power consumption and possibly reduce the sensing performance.

In order to understand the finger effects on the coupled impedance properties, a 2-D cross-sectional analysis model with an entire dual-coil element was established, which had the same parameters as that shown in Fig. 3 and a pixel size of 85 μm and medium of air with relative permittivity 1. The typical simulation results for the electric field distribution are shown in Fig. 5(a) and (b) when finger valleys and finger ridges are in contact respectively. As can be seen in Fig. 5(a), the electric field density in the air decreased gradually when increasing the outward distance. However, Fig. 5(b) shows that when the relative permittivity of the medium changed to a higher value of 80, the resulted field lines became straighter and uniformly spaced. In conclusion, significant difference can be observed during ridge or valley contact to when the medium is air. Furthermore, in order to understand the characteristic of the coupling capacitance in water, the model from Fig. 5 was adopted, but the boundary conditions of the medium have been changed to water with relative permittivity of 80. Similarly as before, the simulation results of the voltage distribution and electrical field trace are shown in Fig. 6 (a) and (b). The results when

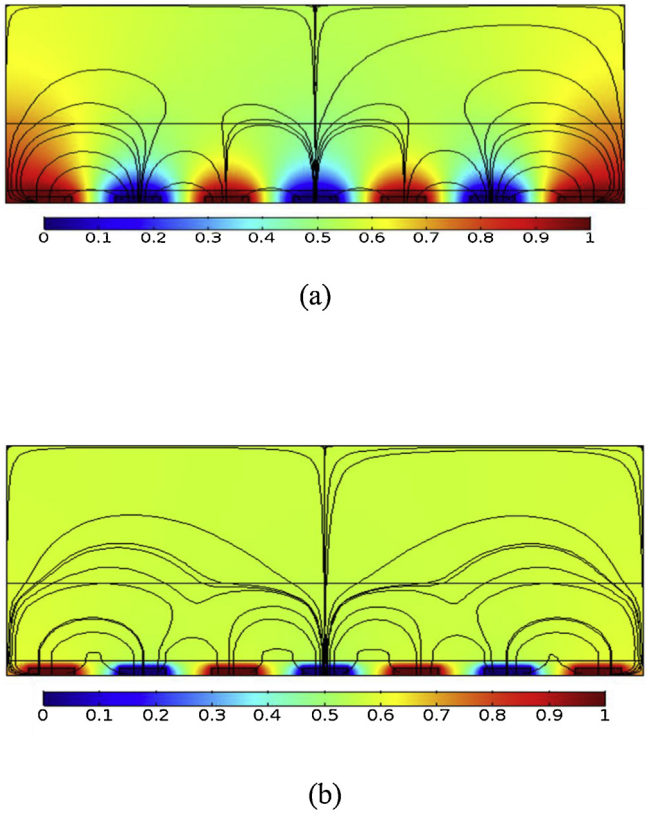

Fig. 12. The simulation result of coupling capacitance with packaging different material: (a) Glass (b) metal.

finger valleys are in contact with the sensor are shown in Fig. (a), and results when finger ridges are in contact are shown in Fig. (b). As can be seen, contrary to the case in air, there is no significant difference in the energy distribution during valley and ridge contacts. All in all, when the capacitive type is placed in air, significant signal differences can be observed between the finger valleys and finger ridges. On the other hand, when placed in a medium of water, coupling capacitive signals differences between the finger valleys and ridges are hard to observe.

The simulation result of the quantitative analysis for coupling capacitance varying with the relative permittivity of the medium is shown in Fig. 7. This result showed that the coupling capacitance increased from 330 pF to 390 pF when the relative permittivity is increased from 20 to 120 with a logarithmic relationship. Furthermore, the same analysis was done for medium of water. In Fig. 8, the simulation results in water of the coupling capacitance with differing finger relative permittivity is shown. When the relative permittivity increased from 20 to 120, the coupling capacitance will increase from 625.6 pF to 848.3 pF.

Similarly, based on the above analysis conditions, the simulation results of the magnetic field were as shown in Figs. 9 and 10. Fig. 9(a) and (b) are the simulated magnetic field strength distributions when the relative permeability is assumed to be 1.0 and 0.4, respectively, and Fig. 10 is the result of the mutual inductance varying with the relative permeability of the medium. A comparison between Fig. 9(a) and 9(b) showed there was no obvious difference. However, Fig. 10 shows that the mutual inductance increased with the relative permeability according to a square relationship. The produced mutual inductance increased from 6.3 nH to 20.8 nH when the relative permeability was within the range of 0.2 and 1.0. These variations changed the output signal of the sensing coil. Since the relative permeability of air and water are both 1, and the typical relative permeability of the finger is 0.4, the working environment

Please cite this article as: S. Lin, M. Hsieh, Y. Huang et al., Usage of the impedance effect of a spiral dual-coil for fingerprint sensor application, Sens. Actuators A: Phys., https://doi.org/10.1016/j.sna.2019.111740

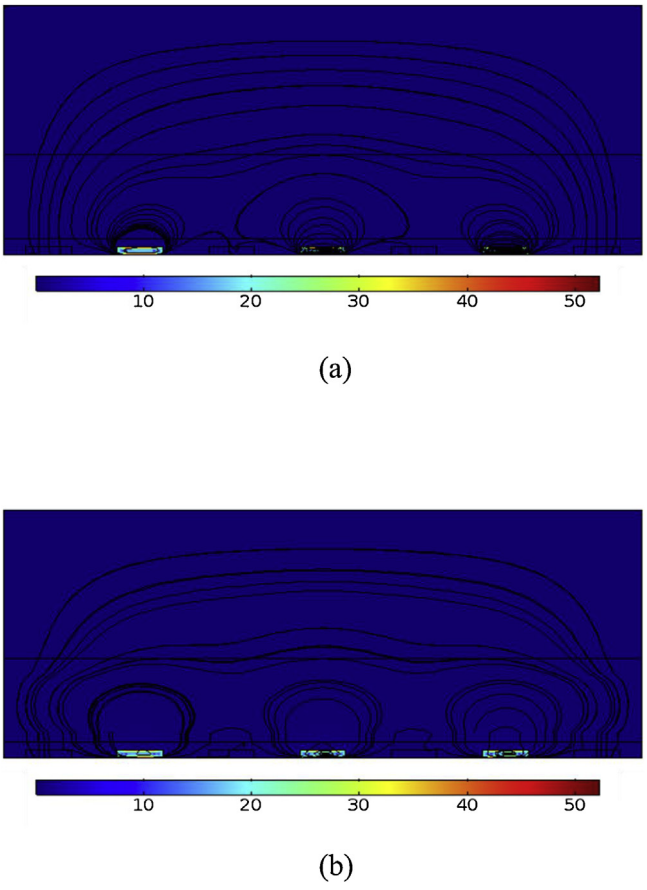

Fig. 13. The simulation result of mutual inductance with packaging different material: (a) Glass (b) metal.

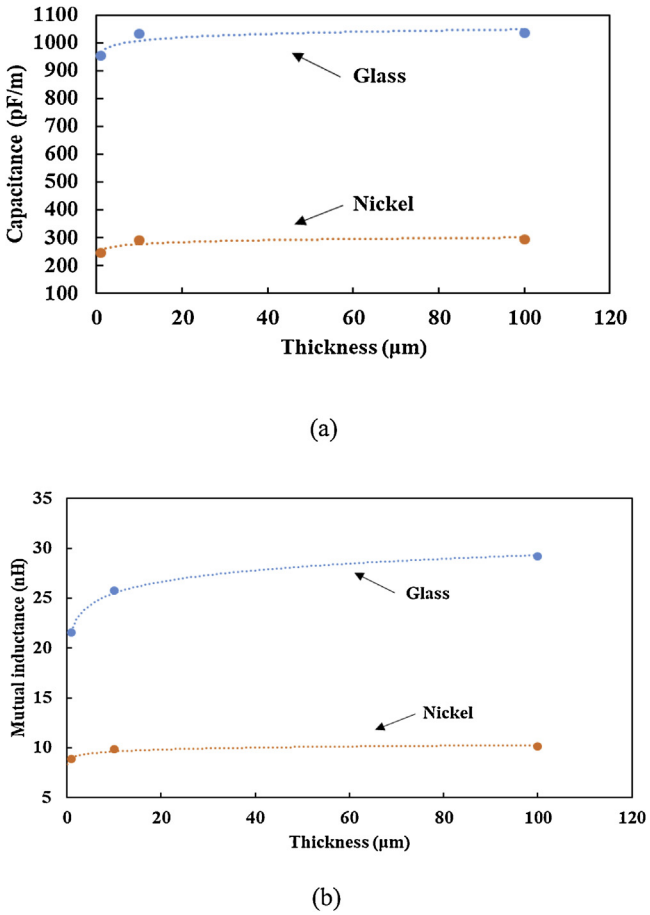

Fig. 14. (a) The relationship between coupling capacitance and thickness with different packaging material and (b) The relationship between mutual inductance and thickness with different packaging material.

of the mutual inductance type in air and water is identical. This indicates that the mutual inductance design's advantage of working in both air and water. It is noted that the higher the relative permittivity and permeability of the passivation layer are, the better is the coupled capacitance and mutual inductance. When the passivation layer thickens, the change in coupled capacitance and mutual inductance during measurement decreases, in turn reducing the sensitivity of the device.

Furthermore, in order to verify the feasibility of the finger with dry and wet properties, the simulation for the finger with different resistance was carried out. The typical simulation results were shown in the Fig. 11(a) to (c). Those results show that there is no obvious variation in the mutual inductance of the dual-coil, when the resistivity of the finger is assumed from 1.0 Ω·m to 1×10^4 Ω·m. For all cases, their mutual inductance values are the same as 11.183 nH, which indicates that the resistivity of the finger does not change the mutual inductance of the dual-coil. This suggests that the proposed sensing concept is significantly less sensitive to humidity than to either capacitive or optical solutions.

In regards to the packaging effect on the coupling capacitive and mutual inductance signals: a metal packaging will have a shielding effect which will cause a signal decay, whereas a glass packaging will not. A COMSOL simulation with a 2D model was conducted to quantitatively characterize the effect of differing packaging material and material thickness on sensor performance i.e. coupling capacitive and mutual inductance. A layer of packaging material (glass or nickel) covers the top of the coils in the model to simulate packaging. Simulation results shown in Fig. 12 (a) and (b) presents the coupling capacitive with packaging material thickness of 10 μm. The result of mutual inductance is also shown in Fig. 13 (a) and (b). In coupling capacitance and mutual inductance, the signal of metal packaging is significantly lower than that of glass. Fig. 14(a) and (b) shows the effect material thicknesses from 0.1 μm to 100 μm has on coupling capacitive and mutual inductance. The coupling capacitance varies from 953.1 pF/m to 1034.9 pF/m under varying glass thicknesses, and 246.0 pF/m to 293.1 pF/m under varying metal thicknesses. Furthermore, the mutual inductance varies from 21.5 nH to 29.2 nH under varying glass thicknesses, and varies from 8.9 nH to 10.2 nH under varying metal thicknesses. This indicates that a metal-based packaging will result in less sensing coil signal, increasing difficulties for circuit design. Therefore, a glass packaging is more suitable for this fingerprint sensor.

Two major design parameters are considered in this design, the thickness and width of the sensing coils. A 3D simulation was conducted through COMSOL to characterize the effects of geometry on sensor performance, under a fixed footprint size of 70 × 70 μm2. Fig.15 (a) and (b) shows the thickness effect on performance under a fixed width of 5 μm. Simulation results show an increase in both C_f and C_p as the thickness of the coils are increased, however, the C_f/C_p ratio is decreasing. This result indicates that the fringing capacitance is less dominant as the thickness of the coil is increased. On the other hand, the mutual inductance increases as the thickness of the coil is increased, and the resistance decreases as the mutual inductance increases. It is thus worthy to keep in mind that the coupling capacitance and mutual inductance have a tradeoff relation.

Next, the simulation of differing sensing coil width is shown in Fig.16 (a) and (b) under fixed thickness 0.3 μm. Since the total

Please cite this article as: S. Lin, M. Hsieh, Y. Huang et al., Usage of the impedance effect of a spiral dual-coil for fingerprint sensor application, Sens. Actuators A: Phys., https://doi.org/10.1016/j.sna.2019.111740

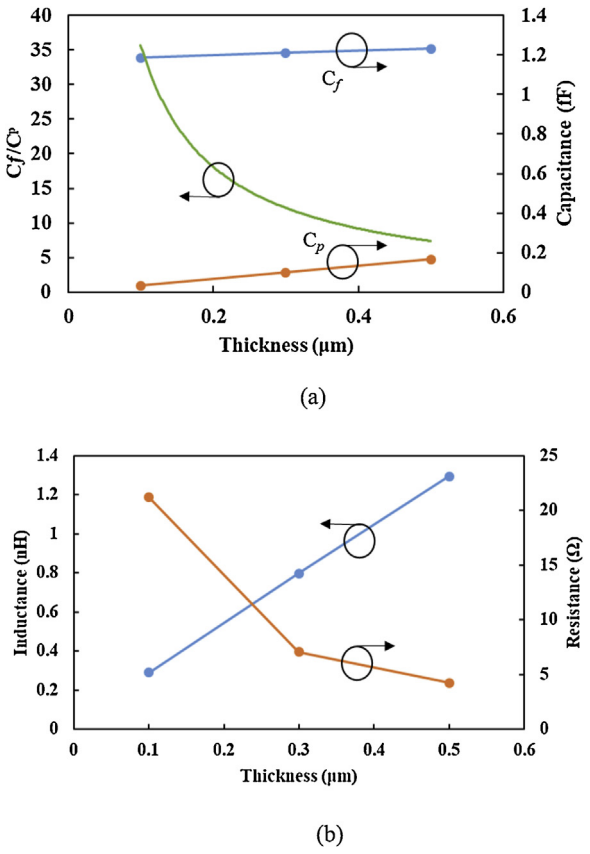

Fig. 15. The simulation results of RLC VS thickness under the condition of 5 μm dual-coil linewidth, (a) capacitance, (b) inductance and resistance.

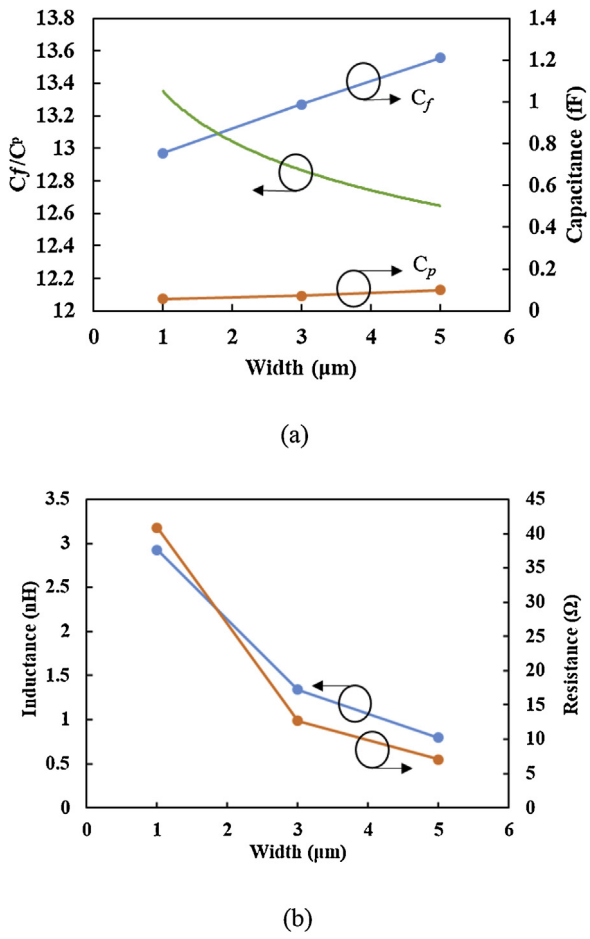

Fig. 16. The simulation results of RLC VS width under the condition of 0.3 μm dual-coil thickness, (a) capacitance, (b) inductance and resistance.

footprint of the coils is fixed, an increase in coil width will simultaneously decrease the coil gap width. Simulation results show that an increase in coil width will lead to an increase in both C_f and C_p, and the C_f/C_p ratio decreases. On the other hand, the mutual inductance and resistivity both decrease as the width of the coil increases. Therefore, it is better to design a smaller coil width for maximizing the coupling effect.

Furthermore, the effects of the shape of the coil have been discussed [19]. Sensing coils with different shapes have different intensities in impedances of capacitances and inductances. In addition, as the arrays become denser, the crosstalk between dual-coils may become more significant. Hence, in order to reduce the crosstalk between different pixels, increase the spacing between distinct pixels can significantly decrease the coupling coefficient between adjacent coils (as refer to the design concern of the RF coil design [20]).

3. Experiment

3.1. Device fabrication

The proposed sensing chip with a spiral dual-coil array was fabricated using a simple silicon-based microfabrication process that had four masks for the patterning electrode, contact windows, coil microstructure, and passivation layers. The schematic of the fabrication process is shown in Fig. 17 and detailed as follows:

(a) An SiO_2 layer was thermally grown on a silicon wafer as an insulation layer.
(b) A photolithography process (mask #1) was implemented to define the pattern of the conductive layer.
(c) Ti/Al (30 nm/300 nm in thickness) layers were deposited by a sputtering process.
(d) The electrical connecting layer was completed by a lift-off process.
(e) An insulation layer of SiO_2 was deposited and patterned by CVD and photolithography processes (mask #2), respectively.
(f) An ICP process was used for the etching window.
(g) A photolithography process (mask #3) was implemented to define the pattern of the dual-coil structure and Ti/Ni (30 nm/300 nm in thickness) layers were then deposited by a sputtering process.
(h) The coil structure was completed by a lift-off process.
(i) A 4 μm photoresist (PR) passivation layer was coated on the coils and then patterned by a photolithography process (mask #4).

A typical fabrication result for a sensing device with a 3×128 array and enlarged views of the dual-coil structure are shown in Fig. 18(a) to 18(c), respectively. Fig. 18(b) shows that the planar dimension of each dual-coil array was about $70 \times 70\ \mu m^2$. The pixel size is $85 \times 85\ \mu m^2$ for the necessary of minimum solution of 300 dpi, allowing feature extraction in fingerprint image detail. Because of the fabrication accuracy, the measured coil's width and gap were 7 μm and 3 μm, respectively, which was slightly different from the original design of 5 μm in both sizes. Fig. 18(c), shows that the entire coil was covered in a photoresist layer and that no obvious defects were observed. It was noted that using high dielectric constant materials such as thin films of SiO_2, Si_3N_4, and SiC to replace the PR passivation layer could provide better electrical isolation.

Please cite this article as: S. Lin, M. Hsieh, Y. Huang et al., Usage of the impedance effect of a spiral dual-coil for fingerprint sensor application, Sens. Actuators A: Phys., https://doi.org/10.1016/j.sna.2019.111740

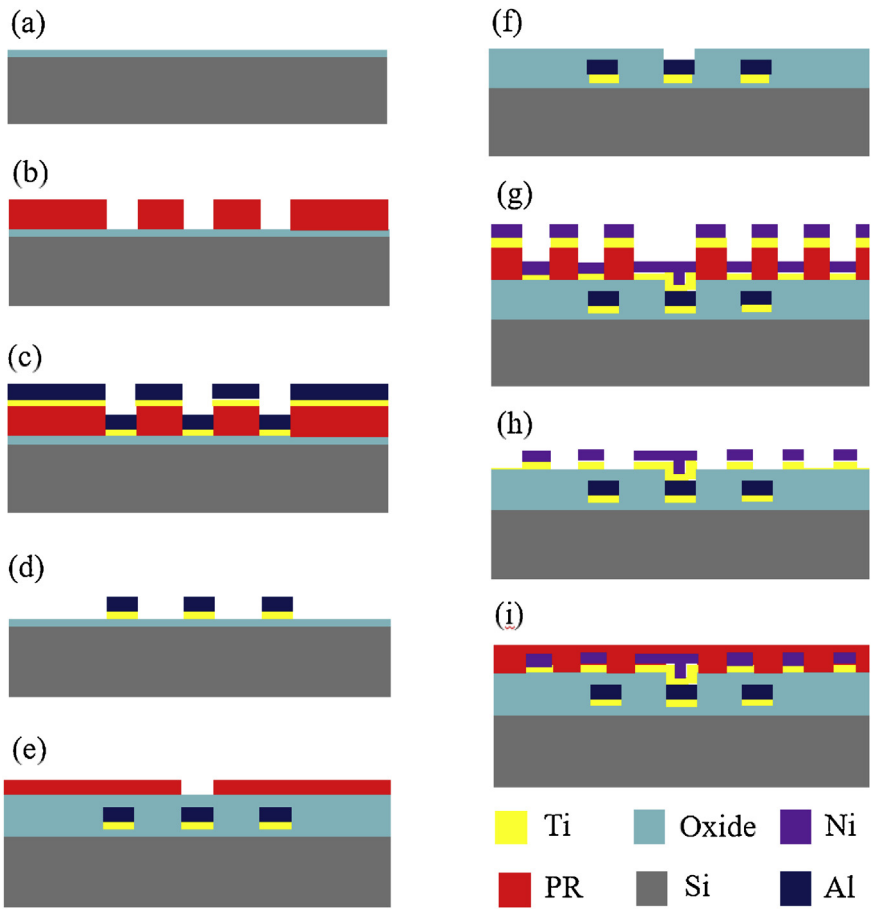

Fig. 17. Fabrication process for the proposed fingerprint-sensing chip.

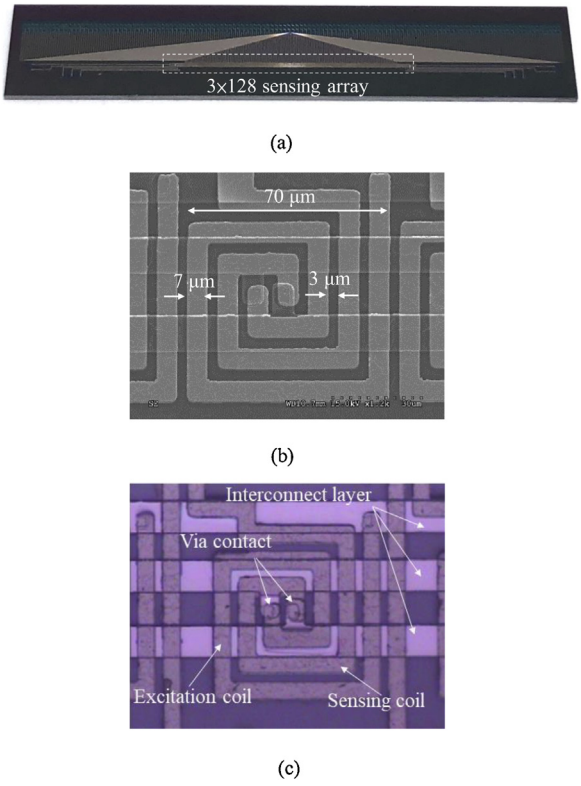

Fig. 18. a) Typical fabrication result for the sensing chip; (b) and (c) SEM and OM images of a single dual-coil.

3.2. Sample testing

The RLC electrical properties of the dual-coil array were first measured using a multimeter and an LCR Meter, as shown in Fig. 19, in which the signal cables were in direct contact with the electrode pads of the sensing chip. A 1.0 $V_{p\text{-}p}$, 100 kHz sine wave was applied as the input signal and the measured impedance model was set as a series C–R circuit because the total resistance was less than 1.0 kΩ. Under these experimental conditions, the equivalent resistance, inductance, and coupling capacitance were sequentially determined as 690 Ω, 8.7 pF, and 4.2 μH, respectively, for a typical case. Furthermore, considering the response characteristics of the coil structure, the time constant (τ) of the RL series circuit can be calculated as 6 ns (i.e. L/R). Since the transient response time of typical RL series circuits is around 5τ, the estimated transient response time is 30 ns. It is noted that the time delay, between the excitation coil and sensing coil, is neglected, due to the gap is only several micrometers.

To understand the basic characterization of mutual inductance, the fabricated dual-coil structure was first operated in the air, using a sine wave input signal and a voltage of 5 $V_{p\text{-}p}$. During the experiment, the sensing chip was directly set in an environment-controlled chamber, with a temperature of 26 ± 0.1 °. The sensing signal was observed on the connected oscilloscope when an excitation signal was input from a function generator. A typical measurement result at a specific driving frequency of 19 MHz is shown in Fig. 20; it clearly shows that the two electrical signals were phase (Ø) shifted by 63.9°.

The inductance performance of the dual-coil array at different driving frequencies was also measured in order to identify the opti-

Please cite this article as: S. Lin, M. Hsieh, Y. Huang et al., Usage of the impedance effect of a spiral dual-coil for fingerprint sensor application, Sens. Actuators A: Phys., https://doi.org/10.1016/j.sna.2019.111740

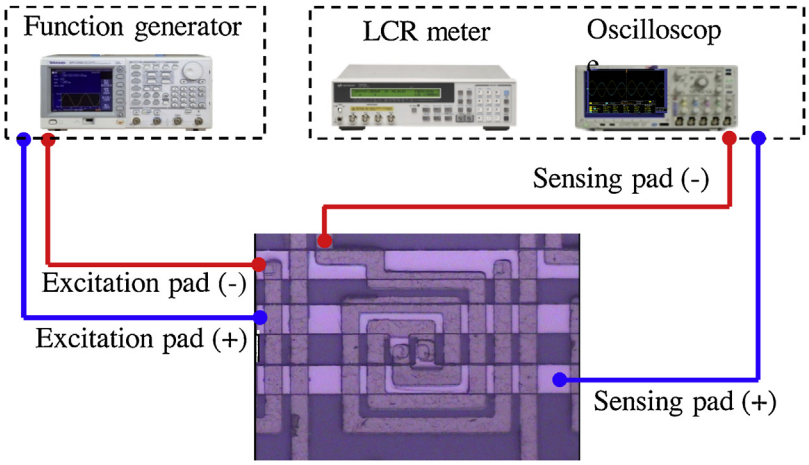

Fig. 19. The basic measurement system with electrical connections.

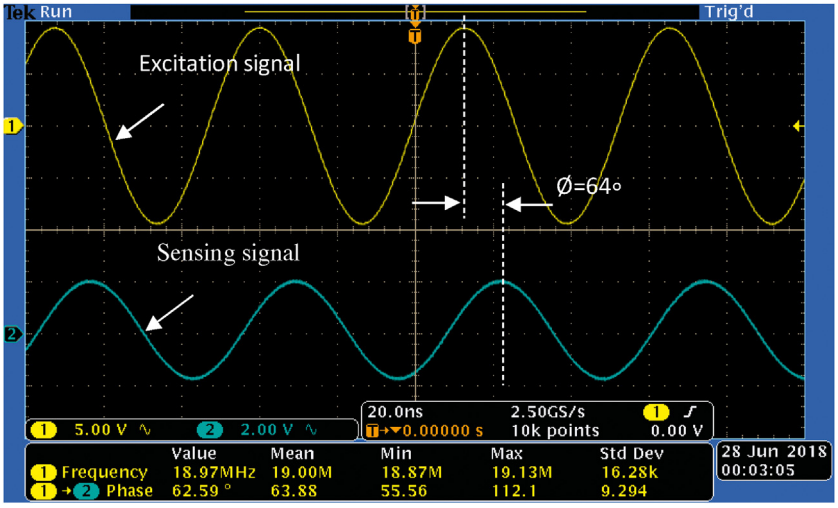

Fig. 20. Typical measurement result with the sensing chip operating in air.

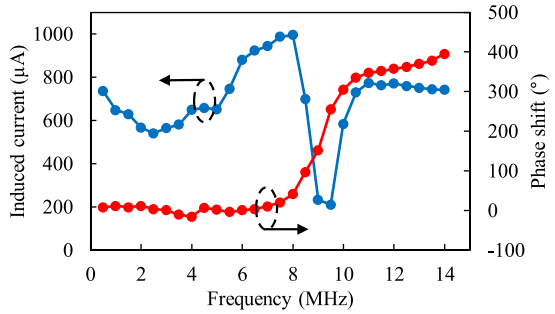

Fig. 21. Induced current and phase shift variations with different driving frequencies.

mal operating conditions. The measured result was as shown in Fig. 21. This figure demonstrates that the resonant frequency was produced at 8 MHz, which resulted in a maximum induced current of about 1 mA and a phase shift of 45.5°. Besides, the sensing signal has a mean voltage of 580 mV with a standard deviation of 16.5 mV, which reveals that the signal-to-noise ratio (SNR) in the time domain is about 35.2. The power consumption is 60.9 μW. Operating at this specific frequency for follow up measurements would be beneficial for reducing current leakage and noise impacts and ensuring better sensing performance.

To create a salt content analogous to the human body, saline solutions with different concentrations were also tested to verify the possibility of quantitative inspection, because salt (NaCl) is an electrolyte and becomes sodium ions (Na^+) and chloride ions (Cl–) when dissolved in water, each of which forms a corpuscle that conducts electricity. At the beginning of this experiment, each saline solution (with the same volume of about 0.1 mm^3) was directly dropped on the tested dual-coil structure, as shown in Fig. 22(a). After applying the same input signal above, the measured results were as shown in Fig. 22(b). These results showed that the phase shift varied with the saline concentration and that the phase difference increased as the concentration increased. This was reasonable because the molar conductivity is the ratio between the conductivity of a solution and its concentration. The greater the number of Na^+ and Cl– ions in the water, the more electricity was conducted; therefore, the higher the conductivity, the greater the phase variation, as implied in the design concept. Under the effect of the 20 wt% saline solutions, the phase shaft was changed from 50.8–52.1 degrees compared to the case of deionized water.

With the pixel array's components working together, the sensing image of a partial fingerprint from a user's swiped finger was reconstructed with a normalized grayscale on the phase variation, as shown in Fig. 23(a), in which the measured maximum variation on the phase shift was 3.8 degrees. For comparison, an imprint image from the same finger is also shown in Fig. 23(b). The two

Please cite this article as: S. Lin, M. Hsieh, Y. Huang et al., Usage of the impedance effect of a spiral dual-coil for fingerprint sensor application, Sens. Actuators A: Phys., https://doi.org/10.1016/j.sna.2019.111740

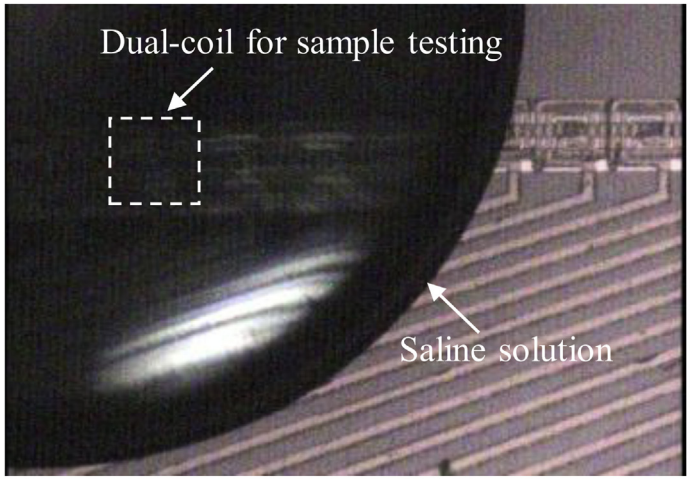

(a)

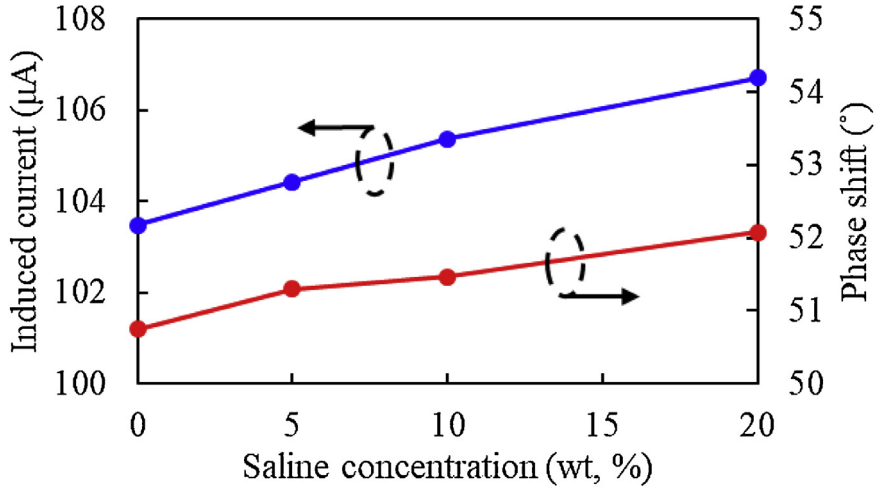

(b)

Fig. 22. a) Top view of the saline solution dropped on the tested dual-coil structure; (b) Variations in the induced current and phase shift with the saline concentration.

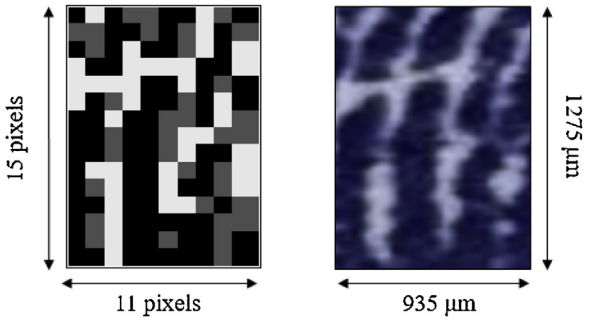

(a) (b)

Fig. 23. a) The measured fingerprint pattern with a normalized grayscale on the phase variation; (b) Image acquired by the fingerprint imprint.

images (both 935 μm × 1275 μm, i.e., 11 × 15 pixels) presented a good match. Most of the white blocks shown in Fig. 21(a) properly reflected the positions of the fingerprint ridges. In the future, using binary images according to a ridge thinning method could achieve a higher fingerprint identification success rate [21]. A fingerprint sensor with high resolution and high sensing performance could also be fabricated by a fine-linewidth CMOS process, due to the CMOS platform may enable more flexibility in the RLC design of the sensor and provide multi-layer stacking capabilities to increase resolution by freeing the originally employed area. Besides, utilizing the design of large sensing arrays and integrating the signal reading circuits with high processing ability, a large sensing image can be obtained, which can further enhance the fingerprint sensing capability of the sensor.

4. Conclusion

This study used silicon-based microfabrication technology to produce a sensing chip with a coplanar dual-coil array that was successfully used to reconstruct a fingerprint image by measuring the phase variation. The spiral dual-coil design increased the variations of the coupling capacitance and mutual inductance, thereby resulting in better sensing performance. The simulation results

Please cite this article as: S. Lin, M. Hsieh, Y. Huang et al., Usage of the impedance effect of a spiral dual-coil for fingerprint sensor application, Sens. Actuators A: Phys., https://doi.org/10.1016/j.sna.2019.111740

showed that the coupling capacitance increased with the relative permittivity with a logarithmic relationship. In addition, the mutual inductance increased with the relative permeability according to a square relationship. The experiment results revealed that a higher medium conductivity resulted in a greater phase variation. Operating at the resonant frequency of 8 MHz, a maximum induced current of 1 mA and a phase shift of 45.5° were obtained. A 11 × 15 pixel-sensing image exhibited a good match with the user's finger pattern. Optimizing the electrical impedance of the dual-coil array and the scale sizes in the dimensions would result in better sensing performance.

Acknowledgment

This study was supported by the Ministry of Science and Technology of Taiwan under grant MOST 106-2221-E-035-054-MY3. The authors appreciate the Precision Instrument Support Center of Feng Chia University, Nano Facility Center of National Chiao Tung University, and the NSC National Nano Device Laboratory (NDL) for providing the fabrication facilities.

References

[1] J.A. Unarab, W.C. Senga, A. Abbasia, A review of biometric technology along with trends and prospects, Pattern Recognit. 47 (2014) 2673–2688.
[2] R. Clodfelter, Biometric Technology in Retailing: Will Consumers Accept Fingerprint Authentication? J. Retail. Consum. Serv. 17 (3) (2010) 181–188.
[3] D. Bhattacharyya, R. Ranjan, F. Alisherov, M. Choi, Biometric authentication: a review, Int. J. U- E- Serv. Sci. Technol. 2 (No. 3) (2009) 13–28.
[4] N.S. Prakash, N. Venkatram, Establishing efficient security scheme in home IOT devices through biometric finger print technique, Indian J. Sci. Technol. 9 (No. 17) (2016) 1–8.
[5] M. Tartagni, R. Guerrieri, A fingerprint sensor based on the feedback capacitive sensing scheme, IEEE J. SolidState Circuits 33 (No. 1) (1998) 133–142.
[6] S. Igaki, S. Eguchi, F. Yamagishi, H. Ikeda, T. Inagaki, Real-time fingerprint sensor using a hologram, Appl. Opt. 31 (No. 11) (1992) 1794–1802.
[7] B. Charlot, F. Parrain, N. Galy, S. Basrour, B. Courtois, A sweeping mode integrated fingerprint sensor with 256 tactile microbeams, J. Microelectromechanical Syst. 13 (No. 4) (2004) 636–644.
[8] J.S. Han, T. Kadowaki, K. Sato, M. Shikida, Fabrication of thermal-isolation structure for microheater elements applicable to fingerprint sensors, Sens. Actuators A Phys. 100 (No. 1) (2002) 114–122.
[9] X. Jiang, H. Tang, Y. Lu, E.J. Ng, J.M. Tsai, B.E. Boser, D.A. Horsley, Ultrasonic fingerprint sensor with transmit beamforming based on a PMUT array bonded to CMOS circuitry, Transactions on Ultrasonics, Ferroelectrics, and Frequency Control 64 (No. 9) (2017) 1401–1408.
[10] S. Shigematsu, H. Morimura, T. Adachi, T. Adachi, K. Machida, A single-chip fingerprint sensor and identifier, IEEE J. SolidState Circuits 34 (No. 12) (1999) 1852–1859.
[11] J.S. Han, Z.Y. Tan, K. Sato, M. Shikida, Thermal characterization of Micro heater arrays on a polyimide film substrate for fingerprint sensing applications, J. Micromechanics Microengineering 15 (No. 2) (2005) 282–289.
[12] S. Memon, M. Sepasian, W. Balachand, Review of finger print sensing technologies, IEEE International Multitopic Conference, Karachi, Pakistan (2008) 226–231, 23-24 Dec.
[13] Y. Lu, H. Tang, S. Fung, Q. Wang, J.M. Tsai, M. Daneman, B.E. Boser, D.A. Horsley, Ultrasonic fingerprint sensor using a piezoelectric micromachined ultrasonic transducer array integrated with complementary metal oxide semiconductor electronics, Appl. Phys. Lett. 106 (26) (2015) 263503 (5pp).
[14] J.F. Mainguet, M. Pégulu, J.B. Harris, Fingerprint recognition based on silicon chips, Future Gener. Comput. Syst. 16 (No. 4) (2000) 403–415.
[15] H.-Y. Tang, Y. Lu, X. Jiang, E.J. Ng, J.M. Tsai, D.A. Horsley, B.E. Boser, 3-d ultrasonic fingerprint Sensor-on-a-Chip, IEEE J. SolidState Circuits 51 (No. 11) (2016) 2522–2533.
[16] W. Li, S. Liao, C. Tsou, A novel sensing chip with Dual-Coil Inductance for determining raw milk quality, Sens. Actuators A Phys. 241 (No. 15) (2016) 96–103.
[17] D. DeHennis, K.D. Wise, A wireless microsystem for the remote sensing of pressure, temperature, and relative humidity, J. Microelectromechanical Syst. 14 (No. 1) (2005) 12–22.
[18] S.K. Yeh, H.C. Chang, W.L. Fang, Development of CMOS MEMS inductive type tactile sensor with the integration of chrome steel ball force interface, J. Micromechanics Microengineering 28 (No. 044005) (2018) 1–11.
[19] S. Liao, W. Li, S. Lin, K. Tang, C. Liou, C. Tsou, A study of the effect of different coplanar dual-coil geometries on the performance of mutual inductance, Sens. Actuators A Phys. 269 (No. 1) (2018) 99–110.
[20] J.H. Mikkelsen, O.K. Jensen, T. Larsen, Measurement and modeling of coupling effects of CMOS on-chip Co-planar inductors, Topical Meeting on Silicon Monolithic Integrated Circuits in RF Systems (2004) 37–40.
[21] J. Zhou, J. Gu, A model-based method for the computation of fingerprints' orientation field, Ieee Trans. Image Process. 13 (No. 6) (2004) 821–835.

Biographies

Shihwei Lin was born in Taipei, Taiwan. He received his B.S. and M.S. degrees in engineering from the Automatic Control Engineering Department, Feng Chia University, Taichung, Taiwan, in 2014 and 2018, He is currently a pH.D. student in the Department of Power Mechanical Engineering, National Tsing Hua University, Taiwan. His research interests include design and implementation of the micro tactile sensor, contact interface design/integration of the micro tactile sensor, and the implementation of fingerprint sensors.

Mingyu Hsieh received the B.S. and M.S. degrees in engineering from the Automatic Control Engineering Department, Feng Chia University, Taichung, Taiwan, in 2015 and 2019, respectively. His current research interests include microelectromechanical systems and micro-LED display system.

Yuanyuan Huang received his BS degree in the Automatic Control Engineering Department, Feng Chia University, Taichung, Taiwan, in 2018. He is currently pursuing the M.S. degree in the Automatic Control Engineering Department, Feng Chia University, Taichung, Taiwan. He is expected to studying PhD. His current research interests include MEMS and micro-LED display system.

Fuchi Shih received his B.S. degree in the Automatic Control Engineering Department, Feng Chia University, Taichung, Taiwan, in 2018. He is currently pursing the M.S. degree in the Automatic Control Engineering Department, Feng Chia University, Taichung, Taiwan. He is expected to studying PhD. His major research is focus on the MEMS and micro-probe integration.

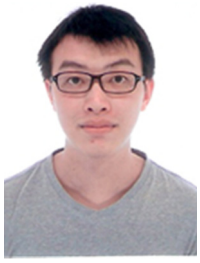

Zihsong Hu received the B.S. degree from the Automatic Control Engineering Department, Feng Chia University, Taichung, Taiwan, in 2018. He is currently pursuing the M.S. degree with the Automatic Control Engineering Department, Feng Chia University, Taichung, Taiwan. His current research interests include microelectromechanical systems and light-emitting packaging.

Weileun Fang was born in Taipei, Taiwan. He received his pH.D. degree from Carnegie Mellon University in 1995. His doctoral research focused on the determining of the mechanical properties of thin films using micromachined structures. In 1995, he worked as a postdoctoral research at Synchrotron Radiation Research Center, Taiwan. He joined the Power Mechanical Engineering Department at the National Tsing Hua University (Taiwan) in 1996, where he is now a Chair Professor as well as a faculty of NEMS Institute. In 1999, he was with Prof. Y.-C. Tai at California Inst. Tech. as a visiting associate. He became the IEEE Fellow in 2015 to recognize his contribution in MEMS area. His research interests include MEMS with emphasis on

Please cite this article as: S. Lin, M. Hsieh, Y. Huang et al., Usage of the impedance effect of a spiral dual-coil for fingerprint sensor application, Sens. Actuators A: Phys., https://doi.org/10.1016/j.sna.2019.111740

micro fabrication/packaging technologies, CMOS MEMS, CNT MEMS, micro optical systems, micro sensors and actuators, and characterization of thin film mechanical properties. He is now the Chief Editor of JMM, the Associate Editor of IEEE Sensors Journal, and the Board Member of IEEE Transactions on Device and Materials Reliability. He served as the member of ISC (International steering committee) of Transducers in 2009–2017, and the ISC chair in 2017-2019. He also served as the General Chair of Transducers Conference in 2017. He was the TPC of IEEE MEMS and EPC of Transducers for many years, and the Program Chair of IEEE Sensors Conference in 2012. He served as the Chief Delegate of Taiwan for the World Micromachine Summit (MMS) in 2008–2012, and the General Chair of MMS in 2012. Prof. Fang has close collaboration with MEMS industries and is now the VP of MEMS and Sensors Committee of SEMI Taiwan.

Chingfu Tsou received the M.S., and pH.D. degrees in power mechanical engineering from National Tsing Hua University (NTHU), Hsinchu, Taiwan, Republic of China, in 1998 and 2003, respectively. Currently, he is a Professor of the Department of Automatic Control Engineering, Feng Chia University, Taiwan, and has more than two years of working experience in the field of MEMS and fingerprint sensor. His research interests include MEMS devices and systems, as well as MEMS/IC packaging technology.

Please cite this article as: S. Lin, M. Hsieh, Y. Huang et al., Usage of the impedance effect of a spiral dual-coil for fingerprint sensor application, Sens. Actuators A: Phys., https://doi.org/10.1016/j.sna.2019.111740